Effect of the electromagnetic environment on the dynamics of charge and phase particles in one-dimensional arrays of small Josephson junctions

2011 EPL 96 47004

(http://iopscience.iop.org/0295-5075/96/4/47004)

A Letters Journal Exploring the Frontiers of Physics

November 2011

EPL, **96** (2011) 47004
doi: 10.1209/0295-5075/96/47004

www.epljournal.org

Effect of the electromagnetic environment on the dynamics of charge and phase particles in one-dimensional arrays of small Josephson junctions

I. L. Ho[1], W. Kuo[2], S. D. Lin[3], C. P. Lee[3], C. T. Liang[4], C. S. Wu[5(a)] and C. D. Chen[1,6]

[1] *Institute of Physics, Academia Sinica - Taipei 115, Taiwan*
[2] *Department of Physics, National Chung Hsing University - 250, Taichung, Taiwan*
[3] *Department of Electronic Engineering, National Chiao-Tung University - Hsinchu 300, Taiwan*
[4] *Department of Physics, National Taiwan University - Taipei 106, Taiwan*
[5] *Department of Physics, National Chang-Hua University of Education - ChangHua 500, Taiwan*
[6] *Department of Physics, National Chen-Kung University - Tainan 701, Taiwan*

received 29 March 2011; accepted in final form 30 September 2011
published online 11 November 2011

PACS 74.40.Kb – Quantum critical phenomena
PACS 74.81.Fa – Josephson junction arrays and wire networks
PACS 74.25.Dw – Superconductivity phase diagrams

Abstract – The effect of the electromagnetic environment on the dynamics of quasi-particles, Cooper pairs and phase particles in one-dimensional arrays of small Josephson junctions is investigated experimentally and theoretically. It is found that the environment enhances the phase ordering and thus suppresses quasi-particle tunneling at high temperature and localization of Cooper pairs at low temperature. The dynamics is studied in the context of phase-charge duality, and the experimental results are quantitatively analyzed in both charge-ordered and phase-ordered regimes. Based on these analyses, a low-temperature phase diagram as well as a finite-temperature crossover phase diagram are constructed and compared to the experimental diagrams.

The competition between phase-order and charge-order in superconducting systems containing small grains has been a long-standing yet fascinating subject of interest [1–6]. Strong inter-grain Josephson coupling locks the phase difference, and the system is in the phase-order regime. Conversely, strong Coulomb interaction suppresses inter-grain charge tunneling, and the system is in the charge-order regime. Upon cooling from high temperature, the competition results in a continuous evolution from superconducting to quasi-reentrant [7] and to insulating regimes provided that the strength of the Josephson coupling is comparable to that of the Coulomb interaction. However, the Josephson coupling and the Coulomb interaction are affected by the presence of external parameters such as quasi-particles [8] and electromagnetic environment [3]. Recent theoretical [9–12] and experimental [13–15] advances revealed the important role of the electromagnetic environment on the fluctuations of phase and charge particles. In the phase-order regime, the electromagnetic environment can be considered to produce dissipation to the phase fluctuations and to support global superconductivity [16], which can eventually lead to dissipative-phase transition [17]. In the charge-order regime, it provides electromagnetic energy needed for virtual tunneling in the Coulomb blockade regime and promotes charge transport [18]. A system consisting of lithographically made small Josephson junctions [19,20] provides a paradigmatic model for studying this competition because here the charging energy can be designed precisely while the Josephson coupling energy can be controlled independently. The one-dimensional Josephson junction array (1D JJA) is an ideal system in which each junction is virtually decoupled from the measurement leads. The superconductor-insulator (SI) transition in 1D arrays of small Josephson junctions was previously explored [21] where the transition is controlled by tuning the Josephson coupling strength. Here, in addition to that, we show that the SI transition can also be tuned by

(a) E-mail: wucs@cc.ncue.edu.tw

changing the impedance of the electromagnetic environment. This is of particular interest as it provides a direct test of the theory of dissipative-phase transition [17].

Using the 1D JJA as an example, in this work we study the effects of a two-dimensional electron gas (2DEG) environment [22,23] on the quasi-reentrant behavior, which reflects directly the dynamics of quasi-particles, phase particles and Cooper pairs. Experimentally, the Josephson coupling strength is varied by an applied magnetic field while the environment strength, which is inversely proportional to the impedance of the underneath 2DEG sheet, is controlled by a pair of side-gates. Being able to tune both the Josephson coupling and the environment strength independently, we mapped out a low-temperature quantum phase diagram [24] in which the region for the quasi-reentrant behavior is identified. The quasi-reentrant behavior is characterized by two resistance turnover temperatures which divide the temperature dependence into three distinct regimes: from low temperature, they are charge-order regime, phase-order regime and quasi-particle dominating regime. Lowering the environment impedance will decrease the upturn temperature and increase the downturn temperature, suggesting enhancement of phase ordering. This, in turn, brings about the suppression of quasi-particle tunneling at high temperature and Cooper-pair blockade at low temperature. By modeling the environment as an ensemble of harmonic oscillators, the two turnover temperatures are calculated as a function of environment and Josephson coupling strengths. Performing the calculations in both charge and phase presentations yields consistent results. Based on these calculations, the low-temperature phase diagram is extended to finite temperatures. This diagram agrees quantitatively with the diagram extracted from the experiment.

1D arrays comprising 100 aluminum SQUIDs (see inset of panel (A_2) in fig. 1) are made on the top of a GaAs/AlGaAs hetero-structure, about 100 nm above the 2DEG sheet. Each SQUID consists of two parallel Josephson junctions with a junction area of $80 \times 180\,\mathrm{nm}^2$, corresponding to a sum junction capacitance C of about 1.5 fF [25] and a charging energy $E_{CP} \equiv 4e^2/2C$ of about $212\,\mu$eV. The arrays are fabricated by standard e-beam lithography and tilted-angle evaporation techniques as addressed in the previous works [19,21]. While the two arrays (denoted as A and B) present here have the same junction area, the junction resistances are different because of the difference in the tunnel barrier thickness. The Josephson coupling energy E_{J0} can be determined by using the Ambegoakar-Baratov relationship, $E_{J0} \equiv (\Delta/2)(R_Q/R_N)$. Here, $R_Q \equiv h/4e^2 \approx 6.45\,\mathrm{k}\Omega$ is the quantum resistance, R_N (6.75 kΩ for A and 7.7 kΩ for B) is the measured normal state resistance of each SQUID (*i.e.* two parallel junctions) and $\Delta = 200\,\mu$eV is the superconducting energy gap. The normal state resistance can be controlled by the oxidation time of the bottom Al electrode before evaporation of the top

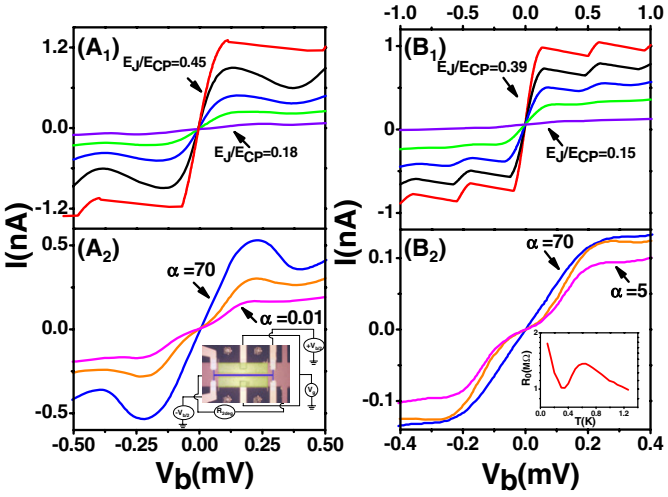

Fig. 1: (Color online) Measured I-V_b characteristics of two arrays A and B. Panels (A_1) and (B_1) show the effects of suppression E_J (from top traces) by the magnetic field when α was tuned to 70, whereas panels (A_2) and (B_2) illustrate the influence of decreasing α (from top traces) by the gate field when the E_J/E_{CP} ratio was tuned to 0.26 and 0.29, respectively. The inset in panel (A_2) is an optical microscope image of the measurement circuit. The inset in panel (B_2) shows the quasi-reentrant behavior measured for array B with $E_J/E_{CP} = 0.29$ and $\alpha = 5$.

Al electrode. Accordingly, E_{J0} of the SQUIDs in arrays A and B is $96.3\,\mu$eV and $83.8\,\mu$eV, respectively. The 2DEG sheet possesses a carrier concentration of about $5 \times 10^{11}/\mathrm{cm}^2$, yielding a sheet resistance $R_\square$ of about 80 Ω at 80 mK. The 1D arrays are placed at the center of a pair of side-gate electrodes which confines the underneath 2DEG sheet into a long strip. The capacitance C_0 between each superconducting island and 2DEG is estimated to be ~ 0.47 fF. The 2DEG structure is similar to that in ref. [23] except that in this work the backgate is replaced by a pair of metal side gates. The two ends of the strip are connected to Au pads via Ohmic contacts for measuring the 2DEG resistance. Through these Ohmic contacts, the zero-bias resistance of the 2DEG strip could be measured using a separated AC lock-in circuit. The gap between the two side-gates is about $5\,\mu$m whereas the width of the 1D SQUID arrays is $1\,\mu$m. The electrons in the strip were depleted by application of a negative voltage on the side-gates, causing an exponential increase in the 2DEG sheet resistance. The arrays were placed in a compartment in a dilution refrigerator equipped with a superconducting magnet, and the electric characterization was performed by using a symmetrical source-meter circuit to minimize any possible pick-up of common mode noises. The zero-bias resistance of the arrays was extracted from the current-voltage (I-V_b) traces taken at varying magnetic fields, side-gate voltages, and temperatures. A perpendicularly applied magnetic field B threading the SQUIDs with loop area A could reduce the Josephson coupling energy to $E_J = E_{J0}\cos(\pi B \times A/\Phi_0)$;

here $\Phi_0 \equiv h/2e$ is the flux quantum. The magnetic field corresponding to a flux quantum in the loop is about 42.5 Gs. The side-gate field has no measurable effect on the arrays themselves with similar E_{J0} and E_{CP} values; this was confirmed separately on other 1D arrays made on bulk silicon chips. For a quantitative analysis, the strength of the environment is defined by a dimensionless conductance, $\alpha \equiv R_Q/R_{2\mathrm{DEG}}$.

Figure 1 illustrates the similarity between the effects of changing E_J and α on the I-V_b characteristics at low temperatures: decreasing E_J and α tends to suppress the critical current and to enhance the Coulomb blockade of Cooper-pair tunneling. However, it is noticed that the influence of α is prominent when the device E_J/E_{CP} value is tuned to be between 0.2 and 0.3 where both phase and charge fluctuations are significant. The small difference in the switching currents shown in panel (B_1) is an indication of the uniformity of the junction parameters in the 1D arrays. The inset in fig. 2(a) shows a low-temperature phase diagram for array A with borders determined by the trend of $R_0(T)$ at $T = T_{min}$ ($T_{min} \approx 100$ mK in the experiment). The phase diagram is largely divided into superconducting region I ($\mathrm{d}R_0/\mathrm{d}T\,|_{T=Tmin} > 0$) and insulating regions II and III ($\mathrm{d}R_0/\mathrm{d}T\,|_{T=Tmin} < 0$). However, here we are interested in region II in which the $R_0(T)$ characteristics exhibit a downturn at T_h and then an upturn at T_l upon cooling. As shown in the inset in panel (B_2) of fig. 1, array B also exhibits a similar behavior. The upturning between T_l and T_{min} is a characteristic known as quasi-reentrant behavior, as shown in fig. 2(a). Figure 2(b) displays the I-V_b as well as the differential conductance ($G_d \equiv \mathrm{d}I/\mathrm{d}V_b$) *vs.* V_b curves at T_h, T_l and T_{min}. We note a clear evolution from governing Josephson tunneling at T_h to onset of Coulomb blockade of Cooper-pair tunneling at T_l and then to strong localization of Cooper pairs at T_{min}. Figure 2(a) also shows the $R_0(T)$ at different α. As α is increased, R_0 at all temperatures decreases; this is attributed to the suppression of phase fluctuations (in the phase-order regime) as well as enhanced higher-order tunneling (in the charge-order regime). Moreover, we find that T_h increases and T_l decreases with increasing α.

For a quantitative analysis of the quasi-reentrant behavior, T_h and T_l are calculated theoretically. The Lagrangian of the system comprises items for an 1D JJA, a 2DEG sheet and the interaction between them and is given by [17,26]

$$\begin{aligned} L_{total} &= L_{JJA} + L_{2DEG} + L_{interaction} = \\ &\frac{1}{2}\sum_{ij} Q_i \left[\left(\hat{C}^{-1}\right)_{ij} + \left(\frac{1}{4e^2}\frac{3\pi}{32\Delta R_{t,ij}}\right)_{ij} \right] Q_j \\ &+ \sum_{\langle i,j\rangle} E_J \left[1 - \cos\left(\varphi_i - \varphi_j\right)\right] + \frac{1}{2}\sum_n (m_n \dot{x}_n^2 \\ &- m_n \omega_n^2 x_n^2) - \sum_{in} F_{in}\left(Q_i, \varphi_i, x_n, \lambda_{in}\right). \end{aligned} \tag{1}$$

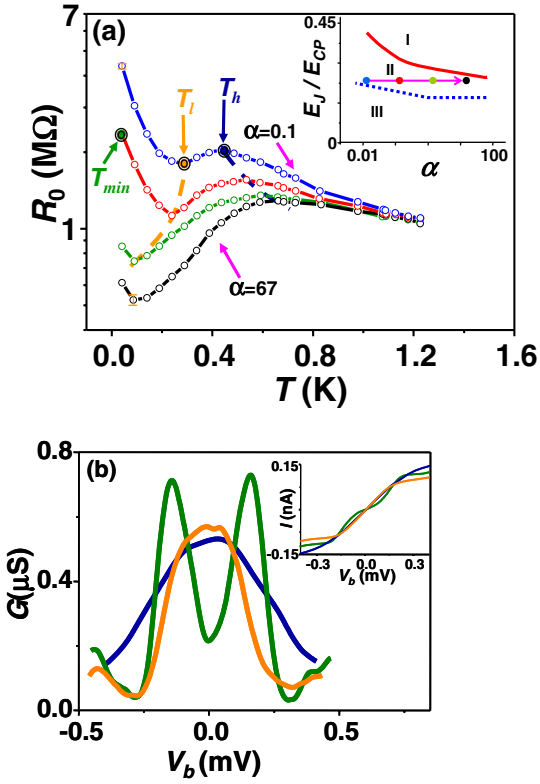

Fig. 2: (Color online) (a) Quasi-reentrant $R_0(T)$ traces at increasing α values for array A with $E_J/E_{CP} = 0.23$. The arrows denote three temperature points, T_h, T_l and T_{min}, and the dashed curves mark α-dependences of T_h (blue) and T_l (orange). The error bars are large for low resistance values and small for high resistance values; shown in the plot are the maximum and minimum error bars. The corresponding α values are indicated in the inset in accordance with the color of the $R_0(T)$ traces. The experimental data are presented as dots in the $R_0(T)$ traces and as crosses in the inset. (b) Differential conductance as a function of bias voltage at $T = T_h$ (blue), T_l (orange) and T_{min} (green). The inset shows I-V_b curves at the corresponding temperatures.

On the right-hand side, the first term describes the array charging energy for Cooper pairs including the renormalization correction to the Cooper-pair Coulomb interaction due to the presence of quasi-particles. The capacitance matrix [18] includes the junction capacitance and the capacitance to the 2DEG strip for diagonal elements and the junction capacitance for off-diagonal elements. In this way, the long-range Coulomb interaction enters automatically. The second term describes the Josephson coupling genergy [26]. The 2DEG environment is represented by an ensemble of harmonic oscillators with resonant (Matsubara) frequencies $\omega_n = 2\pi n k_B T$ [17]. In the last term, λ_{in} describes the coupling strength between superconducting island i and environment oscillator n. For simplicity, we model the 2DEG sheet as an Ohmic environment [27] by applying a constraint [26,28],

$$\sum_n \frac{\pi \lambda_{in}^2}{2\boldsymbol{m}_n} \delta\left(\omega - \omega_n\right) = \boldsymbol{R}_{2DEG}^{-1}. \tag{2}$$

This model is applicable for frequencies below the junction plasma frequency, which is about 300 GHz (or 14 K in temperature).

In the charge presentation, the E_J (*i.e.* the 2nd) term is treated as a perturbation to the charge states and the environment (the 3rd and 4th) terms are taken into account by the $P(E)$ theory [18]. The tunneling rates for Cooper pairs (CPs) and quasi-particles (QPs) are given by the Fermi-Golden rule approximation [18]:

$$\gamma_{CP} = \frac{\pi}{2\hbar} \boldsymbol{E}_J^2 \tilde{\boldsymbol{P}}(\boldsymbol{\delta E}_{ch,CP}), \tag{3a}$$

$$\gamma_{QP} = \frac{1}{\boldsymbol{e}^2 \boldsymbol{R}_t} \int_{-\infty}^{\infty} \mathrm{d}\boldsymbol{E} \int_{-\infty}^{\infty} \mathrm{d}\boldsymbol{E}' \boldsymbol{N}(\boldsymbol{E}) \boldsymbol{N}(\boldsymbol{E}') \boldsymbol{f}(\boldsymbol{E})[1 - \boldsymbol{f}(\boldsymbol{E}')] \times \boldsymbol{P}(\boldsymbol{\delta E}_{ch,QP} + \boldsymbol{E}' - \boldsymbol{E}); \tag{3b}$$

here $\tilde{\boldsymbol{P}}(\boldsymbol{E})$ is the probability function describing the exchange of energy E between environment and Cooper-pairs tunneling. For quasi-particles, this probability function is denoted as $P(E)$. $\boldsymbol{N}(\boldsymbol{E}) = \boldsymbol{\Theta}(|\boldsymbol{E}| - \boldsymbol{\Delta}) |\boldsymbol{E}| / \sqrt{\boldsymbol{E}^2 - \boldsymbol{\Delta}^2}$ is the BCS density of states with a superconducting gap Δ and $\boldsymbol{f}(\boldsymbol{E})$ is the Fermi-Dirac distribution. $\delta E_{ch,CP}$ and $\delta E_{ch,QP}$ are the energy changes associated with the tunneling of the Cooper pairs and quasi-particles, respectively. Although γ_{CP} and γ_{QP} are the tunneling rates for a single junction in the 1D array, the charge statuses of all islands in the array enter via the arguments $\delta E_{ch,CP}$ and $\delta E_{ch,QP}$. In this way, the net tunneling rate Γ for a junction is affected by the tunneling in the rest of the junctions and a correlation in the tunneling events is automatically established. Based on these two equations, the net tunneling rates at varying α and T can be calculated using the Monte Carlo technique and the result for $\vec{\Gamma}_{CP} - \overleftarrow{\Gamma}_{CP}$, $\vec{\Gamma}_{QP} - \overleftarrow{\Gamma}_{QP}$ are displayed in figs. 3(a) and (b), respectively. Details of the calculation technique are given in ref. [29]. $\vec{\Gamma}_{CP} - \overleftarrow{\Gamma}_{CP}$ and $\vec{\Gamma}_{QP} - \overleftarrow{\Gamma}_{QP}$ represent the net tunneling rates for right-moving Cooper pairs and quasi-particles, which can be converted to current by simply multiplying the corresponding Coulomb charges. In panel (a), the temperatures corresponding to the maximum $\vec{\Gamma}_{CP} - \overleftarrow{\Gamma}_{CP}$ are marked by vertical arrows and are identified as T_l. Below T_l, $\vec{\Gamma}_{CP} - \overleftarrow{\Gamma}_{CP}$ decreases due to the Coulomb blockade of the Cooper-pair tunneling. Above T_l, $\vec{\Gamma}_{CP} - \overleftarrow{\Gamma}_{CP}$ is suppressed due to the thermal fluctuations of the island superconducting phase which follows a $\coth(1/T)$-dependence [18] as addressed in the $P(E)$ theory. It is noted that the reentrant behavior exists even in the absence of quasi-particle tunneling (see the black dotted curve). The introduction of quasi-particle tunneling would affect the Cooper-pair tunneling in two ways (cf. the blue solid curve): Firstly, it would reduce the Cooper-pair tunneling rate because CP and QP tunneling are two competing processes as far as the charging effect is concerned. Secondly, it gives rise to an additional dissipation to the phase fluctuations [30] and decreases T_l. On the other hand, since α represents dissipation to the phase fluctuations, reducing α would raise T_l, as indicated by the red arrow. Regarding the downturn dependence at high temperature, T_h can be identified as the temperature at which a sharp increase in the quasi-particle tunneling rate appears, as shown in fig. 3(b). Above T_h, thermally assisted tunneling of quasi-particles gains importance and the transport is described by a simple activation behavior. The effect of the environment on T_h can be understood through the Cooper-pair tunneling rate by comparing the blue and red curves in fig. 3(a). Fast Cooper-pair tunneling, as in the case of large α, would suppress quasi-particle tunneling and raise the T_h value. Based on these calculations, the array resistance at varying temperatures for different α is obtained and displayed in fig. 3(c), which exhibits a good agreement with the measurement results shown in fig. 2(a).

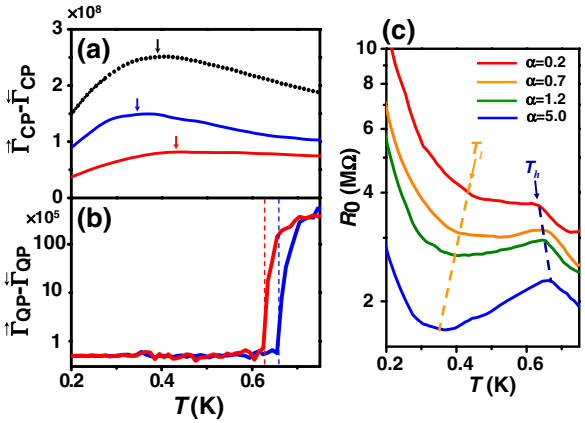

Fig. 3: (Color online) Tunneling rates and zero-bias resistance calculated based on eqs. (3a) and (3b). Temperature dependence of a right-moving Cooper pair tunneling rate (a) and quasi-particle tunneling rate (b) calculated for a 20-junction array with the same junction parameter as array A. The blue and red curves are for $\alpha = 5$ and $\alpha = 0.7$, respectively. The black dotted curve in (a) is obtained by setting $\gamma_{QP} = 0$ and $\alpha = 5$. Three downward arrows in (a) mark the T_l values corresponding to the maximum Cooper-pair tunneling rate. The two vertical dashed lines in (b) corresponding to a sharp increase in the quasi-particle tunneling rate identify the T_h values. (c) Calculated $R_0(T)$ curves for different α. The two dashed lines mark the T_l and T_h values. To compare with the quasi-reentrant behavior shown in fig. 2(a), the E_J/E_{CP} value is set to 0.23.

In the phase presentation, the Lagrangian is analyzed in the context of phase localization in the Josephson potential well [31]. Similar to the Ginzburg-Landau mean-field theory for 2D and 3D junction arrays [32], the 1D JJAs are identified to be in the insulating phase when the phase correlation vanishes: $\langle E_J \cos\varphi_{ij} \rangle = 0$. The presence of the environment (*i.e.* $\alpha \neq 0$) introduces an effective reduction to E_{CP} by a factor of $\sqrt{1 + \alpha \boldsymbol{E}_{CP}/2\pi\omega_n}$. For $T \to 0$, as

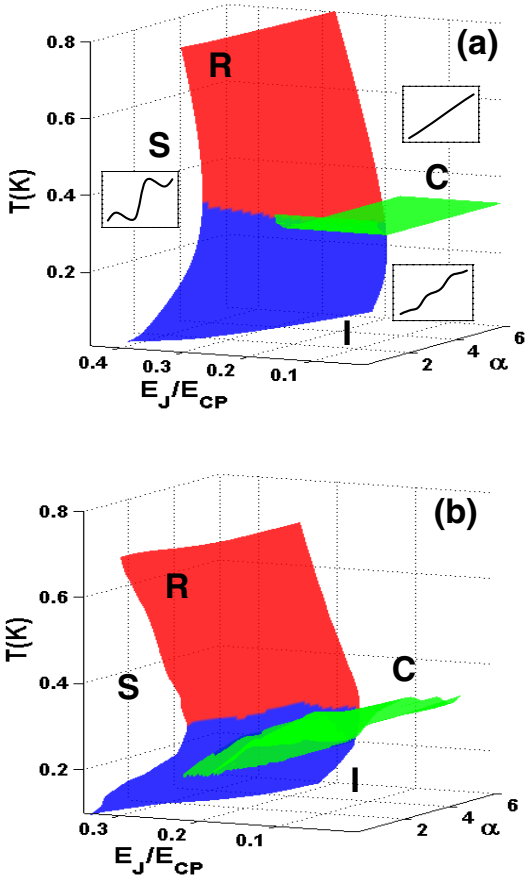

Fig. 4: (Color online) (a) Theoretical and (b) experimental crossover phase diagrams. The border surfaces are presented by different colors: blue for T_l, red for T_h and green for T_m. The border surfaces divide the diagram into 4 regions: superconducting (S), insulating (I), resistive (R) and conductive (C). Insets in (a) are schematic curves illustrating typical I-V_b characteristics in S, I and R/C regions. The projection of the intercept between T_l and T_h border surfaces onto the (E_J/E_{CP}, α)-plane is identical to the blue dashed border shown in the inset of fig. 2(a).

α increases, the effective E_J/E_{CP} value is increased and can be brought across a critical value $(E_J/E_{CP})^*$. This gives rise to an insulator-to-superconductor transition, as illustrated by the red border in the low-temperature phase diagram shown in the inset of fig. 2(a). This is in quantitative agreement with the predication [28] that for $T \to 0$ the border follows the relations $(E_J/E_{CP})^* \alpha = 2$ for $\alpha \gg 1$ and $(E_J/E_{CP})^* = 0.5$ for $\alpha \ll 1$. In the $T \to 0$ plane of the diagram, the SI phase transition is driven by changing E_J (along the E_J/E_{CP} direction) and by changing the dissipation (along the α direction). For $T > 0$, it is found that $\langle E_J \cos \varphi_{ij} \rangle = 0$ has a double root for (E_J/E_{CP}, α) located in a region which coincides with the quasi-reentrant region II defined in the low-temperature phase diagram. The two roots are identified as T_h and T_l. When plotted as a function of (E_J/E_{CP}, α), T_h and T_l form a curled border surface, as displayed in fig. 4(a). This surface indicates the crossover between different regions: a high-temperature resistive region, an intermediate superconducting region and a low-temperature insulating region. For a comparison, fig. 4(b) shows an experimental crossover phase diagram. This diagram can also be understood in charge presentation: For $T > T_h$, the increased quasi-particle tunneling suppresses the phase correlation and the array is pushed toward the resistive region. For $T < T_l$, Cooper pairs are more localized, resulting in strong fluctuations of phase and the array is thus moved toward the insulating region.

Outside the quasi-reentrant region, we show an additional horizontal crossover surface (shown in green), which is referred to as T_m. This surface separates the diagram into a low-temperature "insulating" region and a high-temperature "conductive" region. The experimental criterion for T_m is the appearance of a dip structure in the differential conductance ($G_d \equiv \mathrm{d}I/\mathrm{d}V_b$) *vs.* V_b curve at the zero-bias point; see, *e.g.*, orange and green traces in fig. 2(b). Within our measurement resolution, T_m seems to overlap with the T_l surface. The T_m surface as a function of E_J/E_{CP} and α can also be calculated in the charge presentation addressed above and the result is shown in fig. 4(a). The calculated Cooper-pair current shows a power-law dependence on V_b as $I \sim V_b^a$ at low bias voltages, and a border given by $a = 1$ separates the regions of bound charges ($a > 1$) and free charges ($a \leqslant 1$) [31], which correspond to the insulating and conductive regions, respectively.

In summary, the effect of electromagnetic environment on the dynamics of charge and phase particles is studied by analyzing the quasi-reentrant behavior. By modeling the environment as an ensemble of harmonic oscillators, we calculated a finite-temperature crossover phase diagram, which agrees quantitatively with the experimental results. This study provides a leap toward understanding the effect of the electromagnetic environment on the phase-charge duality.

* * *

Fruitful discussions with H.-J. Lee, S.-I. Lee and B. Altshuler are gratefully acknowledged. This research was funded by the National Science Council of Taiwan under contract Nos. NSC 98-2112-M-001-023-MY3 and NSC 99-2112-M-018-004-MY3. Technical support from NanoCore, the Core Facilities for Nanoscience and Nanotechnology at Academia Sinica, is acknowledged.

REFERENCES

[1] Dubi Y., Meir Y. and Avishai Y., *Nature*, **449** (2007) 876.
[2] Chow E., Delsing P. and Haviland D. B., *Phys. Rev. Lett.*, **81** (1998) 204.
[3] Fazio R. and Van Zant H., *Phys. Rep.*, **355** (2001) 235.

[4] Efetov K. B., *Sov. Phys. JETP*, **51** (1980) 1015.
[5] Feigel'man M. V., Korshunov S. E. and Pugachev A. B., *JETP Lett.*, **65** (1997) 566.
[6] Pop I. M., Protopopov I., Lecocq F., Peng Z., Pannetier B., Buisson O. and Guichard W., *Nat. Phys.*, **6** (2010) 589.
[7] "Quasi-reentrant" is a term coined following the early works of Orr B. G., Jaeger H. M. and Goldman A. M., *Phys. Rev. B*, **32** (1985) 7586; Jaeger H. M., Haviland D. B., Orr B. G. and Goldman A. M., *Phys. Rev. B*, **40** (1989) 182. It should be noted that quasi-reentrance is not strictly a 1D effect.
[8] Kampf A. and Schön G., *Phys. Rev. B*, **36** (1987) 3651.
[9] Lutchyn R. M., Galitski V., Refael G. and Sarma S. D., *Phys. Rev. Lett.*, **101** (2008) 106402.
[10] Wagenblast K. H., Otterlo A. V., Schön G. and Zimányi G. T., *Phys. Rev. Lett.*, **79** (1997) 2730.
[11] Goswami P. and Chakravarty S., *Phys. Rev. B*, **73** (2006) 094516.
[12] Lobos A. M. and Giamarchi T., *Phys. Rev. B*, **84** (2011) 024523.
[13] Corlevi S., Guichard W., Hekking F. W. J. and Haviland D. B., *Phys. Rev. Lett.*, **97** (2006) 096802.
[14] Miyazaki H., Takahide Y., Kanda A. and Ootuka Y., *Phys. Rev. Lett.*, **89** (2002) 197001.
[15] Penttilä J. S., Parts Ü., Hakonen P. J., Paalanen M. A. and Sonin E. B., *Phys. Rev. Lett.*, **82** (1999) 1004.
[16] Bobbert P. A., Fazio R., Schön G. and Zaikin A. D., *Phys. Rev. B*, **45** (1992) 2294.
[17] Caldeira A. O. and Leggett A. J., *Ann. Phys. (N.Y.)*, **149** (1983) 374.
[18] Ingold G. L. and Nazarov Yu V., in *Single Charge Tunneling*, edited by Grabert H. and Devoret M. H. (Plenum Press, New York and London) 1992, Chapt. 2, pp. 21–107.
[19] Lotkhov S. V., Bogoslovsky S. A., Zorin A. B. and Niemeyer J., *Phys. Rev. Lett.*, **91** (2003) 197002.
[20] Chen C. D., Delsing P., Haviland D. B., Harada Y. and Claeson T., *Phys. Rev. B*, **51** (1995) 15645.
[21] Kuo W. and Chen C. D., *Phys. Rev. Lett.*, **87** (2001) 186804.
[22] Kycia J. B., Chen J., Therrien R., Kurdak C., Campman K. L., Gossard A. C. and Clarke J., *Phys. Rev. Lett.*, **87** (2001) 017002.
[23] Rimberg A. J., Ho T. R., Kurdak C. and Clarke J., *Phys. Rev. Lett.*, **78** (1997) 2632.
[24] Refael G., Demler E., Oreg Y. and Fisher D. S., *Phys. Rev. B*, **75** (2007) 014522.
[25] This value was estimated assuming a specific capacitance of $45\,\mathrm{fF}/\mu\mathrm{m}^2$, see Delsing P., Claeson T., Likharev K. K. and Kuzmin L. S., *Phys. Rev. B*, **42** (1990) 7439.
[26] Chakravarty S., Ingold G. L., Kivelson S. and Luther A., *Phys. Rev. Lett.*, **56** (1986) 2303.
[27] Wilhelm F. K., Schön G. and Zimány G. T., *Phys. Rev. Lett.*, **87** (2001) 136802.
[28] Fisher M. P. A., *Phys. Rev. Lett.*, **57** (1986) 885.
[29] Ho I. L., Lin M. C., Aravind K., Wu C. S. and Chen C. D., *J. Appl. Phys.*, **108** (2010) 043907.
[30] Herrero C. P. and Zaikin A. D., *Phys. Rev. B*, **65** (2002) 104516.
[31] Panyukov S. V. and Zaikin A. D., *J. Low Temp. Phys.*, **75** (1989) 361.
[32] Fazio R. and Schön G., *Phys. Rev. B*, **43** (1991) 5307.